JACS
JOURNAL OF THE AMERICAN CHEMICAL SOCIETY

Article

pubs.acs.org/JACS

Supergelation via Purely Aromatic $\pi-\pi$ Driven Self-Assembly of Pseudodiscotic Oxadiazole Mesogens

Aneesh P. Sivadas,[†] N. S. Saleesh Kumar,[†] Deepak D. Prabhu,[†] Shinto Varghese,[†] S. Krishna Prasad,[‡,*] D. S. Shankar Rao,[‡] and Suresh Das*[,†]

[†]Photosciences and Photonics Section, Chemical Sciences and Technology Division, National Institute for Interdisciplinary Science and Technology (NIIST) and Network of Institutes for Solar Energy, Council of Scientific and Industrial Research (CSIR), Trivandrum 695 019 India

[‡]Centre for Soft Matter Research, Jalahalli, Bangalore 560 013 India

Supporting Information

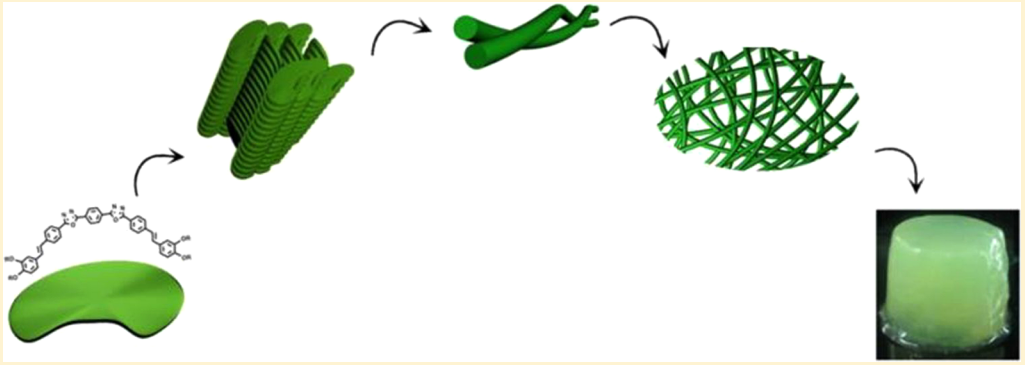

ABSTRACT: A series of highly luminescent oxadiazole-based stilbene molecules (OXD4, OXD8, OXD10, and OXD12) exhibiting interesting enantiotropic liquid crystalline and gelation properties have been synthesized and characterized. The molecules possessing longer alkyl substituents, OXD10 and OXD12, possess a pseudodisc shape and are capable of behaving as supergelators in nonpolar solvents, forming self-standing gels with very high thermal and mechanical stability. Notably the self-assembly of these molecules, which do not possess any hydrogen-bonding motifs normally observed in most reported supergelators, is driven purely by π-stacking interactions of the constituent molecules. The *d*-spacing ratios estimated from XRD analysis of OXD derivatives possessing longer alkyl chains show that the molecules are arranged in a columnar fashion in the mesogens and the self-assembled nanofibers formed in the gelation process.

INTRODUCTION

The spontaneous generation of ordered superstructures with well-defined functional properties from molecules randomly dispersed in a medium requires a molecular level intelligence which will drive the self-assembly in a desired manner.[1] A critical understanding of the weak forces that drive self-assembly is essential for providing structural features to molecules which can impart them with such intelligence. Molecules displaying liquid crystalline behavior (mesogens) in bulk or in the solution phase are ideal candidates for investigating such behavior because of their propensity to form aggregates in an organized manner.[2] A class of self-assembled materials which has attracted special attention in recent years is gels, in view of their potential use in a variety of applications including organic photovoltaics, as templates for inorganic nanostructures and in controlled release systems.[3] Of particular interest are supergelators which can lead to strong self-standing gels, can be molded into any shape, and can undergo self-healing when damaged.[4] A common structural feature among molecules which form supergelators is the presence of strong hydrogen bonding moieties such as amides, polypeptides, and sugar.[5] Molecules without such hydrogen bonding units which can act as supergelators have hitherto not been reported and hence development of such systems can vastly enhance the scope of designing this class of materials and remains a major challenge.

Herein, we report on the supergelating properties of 1,3,4-oxadiazole derivatives capable of self-assembling into columnar architectures in both bulk and in solution (Chart 1). Based on XRD and NMR of the aggregates we could show that the capability of this class of molecules to form unusually strong self-standing gels could be attributed to purely intermolecular $\pi-\pi$ interactions between the oxadiazole-based mesogenic molecules.

Received: January 25, 2014
Published: March 14, 2014

   dx.doi.org/10.1021/ja500607d | *J. Am. Chem. Soc.* 2014, 136, 5416−5423

Chart 1

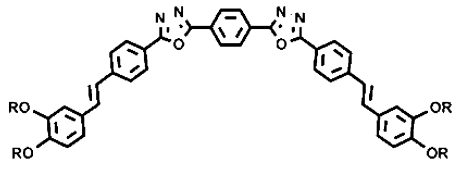

OXD1: R = CH_3 OXD4: R = C_4H_9

OXD6: R = C_6H_{13} OXD8: R = C_8H_{17}

OXD10: R = $C_{10}H_{21}$ OXD12: R = $C_{12}H_{25}$

RESULTS AND DISCUSSION

The oxadiazole derivatives were synthesized by a multistep process,[6] and their structures were established by FTIR, ^1H and ^{13}C NMR, HRMS, and MALDI-TOF mass spectrometry. Details of the synthetic procedures and spectral characterization data of the derivatives are provided in the Supporting Information.

Liquid crystalline properties of all the derivatives were investigated in detail. Preliminary characterization of the different phases was made by studying their optical polarizing microscopic (OPM) textures and confirmed by differential scanning calorimetric (DSC) analyses (Figure S1). All the derivatives exhibited liquid crystalline behavior with the exception of OXD1 and OXD6. While OXD4 exhibited a smectic phase, the longer chain derivatives (OXD8, OXD10, and OXD12) possessed columnar mesophases. For OXD4, the smectic A (Sm_A) phase was seen over a range of 7 °C in the heating cycle and a slightly larger range of 12 °C in the cooling cycle. The presence of columnar organization for OXD8, OXD10, and OXD12 was evident from the X-ray diffraction (XRD) pattern (Figure 1). For OXD8, in the heating cycle, a columnar phase (Col_1) was observed at a temperature of 195

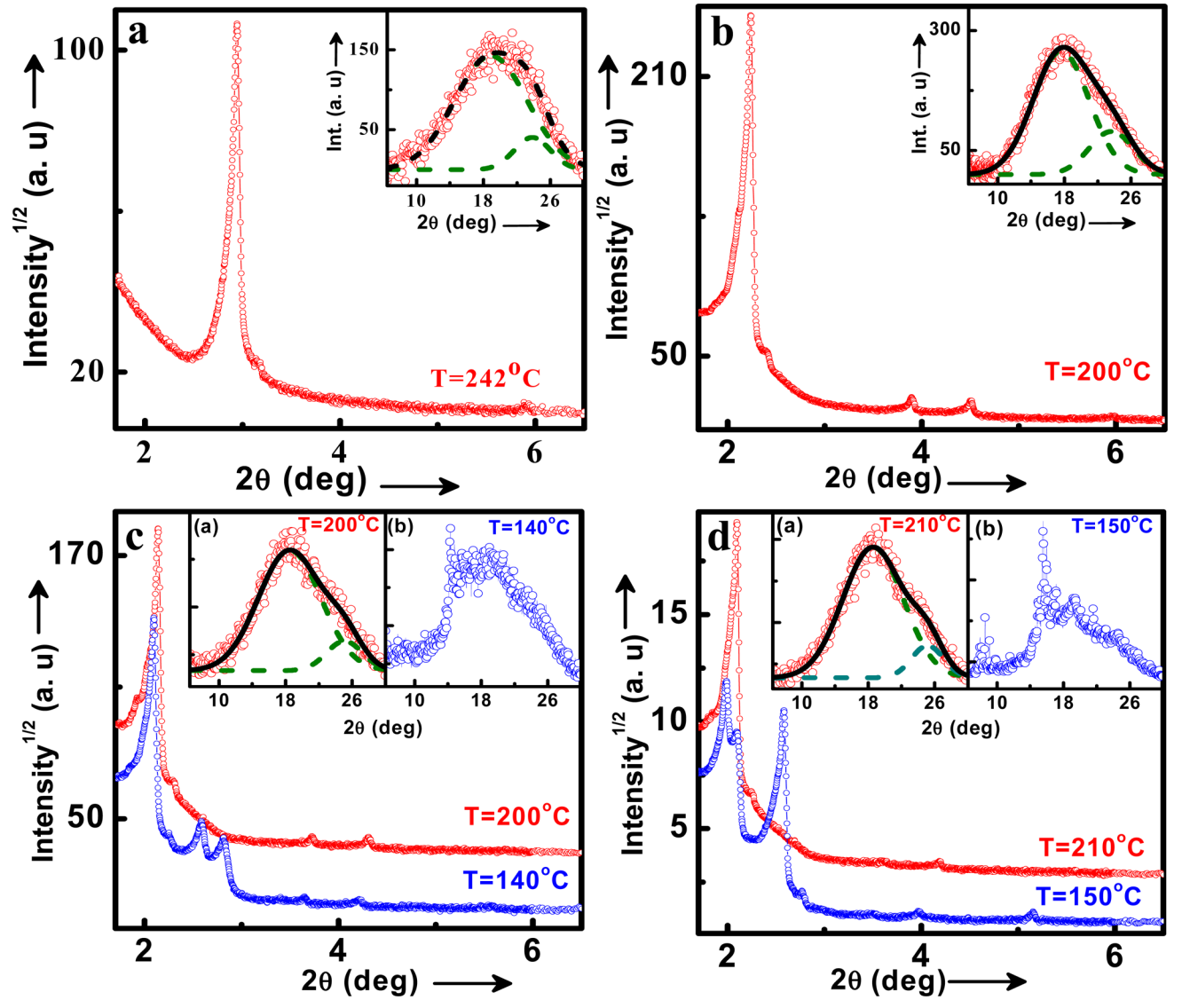

Figure 1. XRD scans for OXD series. The low angle region is shown in the main panel and the wide angle portion in the inset. In the inset, the thick solid line represents the full fit, the individual contributions of which are shown as dashed lines. XRD pattern of (a) OXD4 at 242 °C; (b) OXD8 at T = 200 °C; and (c) OXD10 at two different temperatures. The inset depicts the wide angle region of the diffraction pattern in (a) Col_h and (b) Col_{ob} phases. (d) XRD pattern of OXD12 at two different temperatures. The inset depicts the wide angle region of the diffraction pattern in (a) Col_h and (b) Col_{ob} phases.

dx.doi.org/10.1021/ja500607d | J. Am. Chem. Soc. 2014, 136, 5416−5423

Table 1. X-ray Diffraction Data of the Mesophases of OXD10, Presenting the Measured and Calculated Spacing, Miller Indices, and Lattice Dimensions[a]

transition temperatures [°C] (ΔH [kJ mol^{-1}])	packing motif	d_{meas} [A°]	d_{calc} [A°]	hk	lattice parameters
		41.26	41.19	1 0	a = 47.6 Å at 200 °C
		23.73	23.78	1 1	
	Col_h	20.54	20.60	2 0	
		4.80 (d)			
		3.55 (d)			
Cr_1 108 (7.6) Col_2 167 (21.3) Col_1 233 (3.9) I		42.11	42.00	1 0	a = 43.9 Å b = 35.8 Å γ = 73.0° at 140 °C
		34.23	34.21	0 1	
		31.42	31.40	1 1	
I 232 (3.9) Col_1 160 (0.64) Col_2 152 (19.4) Cr_2 106 (8.6) Cr_1		24.24			
		21.02	21.00	2 0	
		15.90	15.94	−2 1	
	Col_{ob}	13.65	14.00	3 0	
		6.19	6.28	5 5	
		5.66	5.82	6 5	
		4.45	4.49	7 7	
		5.64	5.49	8 2	
		4.67	4.59	8 6	
		4.30 (d)			

[a]Cr = crystalline phase; Col_h = columnar hexagonal mesophase; and Col_{ob} = oblique columnar mesophase.

°C which transformed to the isotropic phase at 220 °C (Table S1). In the cooling cycle, the sample exhibited an isotropic to Col_1 transition at 218 °C and crystallization at 184 °C. In contrast to OXD8, both OXD10 and OXD12 showed two columnar OXD10 mesophases Col_1 and Col_2. For OXD10, the Col_2 and Col_1 phases appeared at 108 and 167 °C, respectively, in the heating cycle and at 160 and 233 °C in the cooling cycle. A similar behavior was observed for OXD12. The thermal phase transitions and their enthalpy values for the OXD series are tabulated (Tables 1 and S1). Detailed identification of the columnar phases for the different samples was carried out by studying their temperature-dependent XRDs.

XRD measurements have been performed on all the four compounds exhibiting liquid crystalline phases, and the results of the measured and calculated spacing, miller indices and lattice dimensions are summarized in Tables 1 and S1. Figure 1a shows the XRD profile of the mesophase of OXD4. Two sharp peaks, one very strong and the other quite weak, are seen at low angles, and a single diffuse peak is seen at wide angles. The spacing of low angle peaks is in the ratio of 1:2. The d_1/L ratio of 0.84, where d_1 is the spacing of the lowest angle peak and L = 35.8 Å is the average length of the molecule, in its bow form, as determined from a molecular model (Figure S2b), indicates the phase to be a layered smectic A phase.

This feature is corroborated by the OPM textures which indicated sharp fan-shaped features (Figure S1a,b). The diffuse maximum in the wide angle region needs a special mention. A proper peak profiling of the data required two Lorentzian expressions, a feature consistent with the behavior of the other compounds studied here. This is however not a common feature in smectic phases but observed normally only in cases where the bulkiness of the two terminal chains are substantially different.[7] Since the terminal chains on either side of the central core are identical in the present case, the reason for such a feature must be different; this aspect is discussed later.

The XRD profiles for OXD8, OXD10, and OXD12 exhibited multiple low angle peaks whose spacing ratios do not conform to layer ordering. For OXD8 (Figure 1b) the inverse of the spacing for four low angle peaks was in the ratio of $1:\sqrt{3}:\sqrt{4}:\sqrt{7}$, which can be identified to be arising from a hexagonal lattice of a columnar structure and indexed as the (10), (11), (20), and (21) reflections, with a lattice dimension of a = 45.4 Å (Table S1). The wide angle region exhibited a broad maximum that can be resolved into two diffuse peaks with spacing of ∼5.0 and 3.8 Å. The former represents the separation between the molten alkyl chains of the molecules along the stacking direction of a column and is observed as a rule in all fluid columnar structures. The second diffuse peak, observed in molecules of disc-like shape, arises due to the possibility of closer stacking of the aromatic cores than the peripheral chains. Thus, such an observation in the present case of nondiscoid molecules is somewhat surprising.

As mentioned earlier OXD10 and OXD12 exhibited two mesophases. The high-temperature phase denoted as Col_1, displayed an XRD pattern which is identical to that shown by the columnar phase of OXD8. The inverse of the spacing for three low angle peaks being in the ratio of $1:\sqrt{3}:\sqrt{4}$ and indexed as the (10), (11), and (20) reflections from a hexagonal columnar structure with a lattice dimension of a = 47.6 and 48.8 Å for OXD10 and OXD12, respectively (Tables 1 and S1). The low-temperature Col_2 phase of both the materials presented a dramatic change in the X-ray pattern, with numerous sharp reflections spread over the entire angular range covered, indicating a well-ordered structure (Figure 1c,d). The presence of the two diffuse reflections at ∼5 and 3.8 Å confirms the fluid nature of the phase. Even a cursory inspection of the first three low-angle sharp reflections ruled out, as expected, the hexagonal lattice.

Detailed indexed analysis, aided by the presence of a number of reflections, brings out the tilted nature of the columnar stacking, with the lattice parameters of a = 43.9 Å, b = 35.8 Å, and γ = 73° and a = 45.5 Å, b = 42.9 Å, and γ = 78.3° for OXD10 and OXD12 compounds, respectively. The reduction in the lattice parameters from the Col_1 to Col_2 phase is in conformity with the oblique nature of the Col_2 phase. In the hexagonal phase (Col_1) of both the materials the lattice dimension comes out to be about 0.95 times the molecular diameter as determined from the molecular model (Figure S2).

dx.doi.org/10.1021/ja500607d | J. Am. Chem. Soc. 2014, 136, 5416−5423

For OXD10 and OXD12 the chains are long enough to give it a pseudodisc appearance. Thus the possible explanation for the presence of the second diffuse peak is that the central oxadiazole units must be strongly interacting with aromatic rings of other molecules ($\pi-\pi$ stacking) in the smectic as well as the columnar phases.

The OXD series showed a strong tendency to form aggregates in solutions with the higher homologues forming stable gels in organic solvents such as *n*-decane, hexadecane, cyclohexane, hexane, *n*-butanol, and toluene (Table S2). It was observed that for OXD8 to OXD12 the critical gelation concentration was very low; for example, in *n*-decane, the CGC for OXD10 was 0.35 wt %. Molecules capable of gelating solvents at concentrations lower than 1 wt % are generally classified as super gelators.[8] Figure 2 depicts various character-

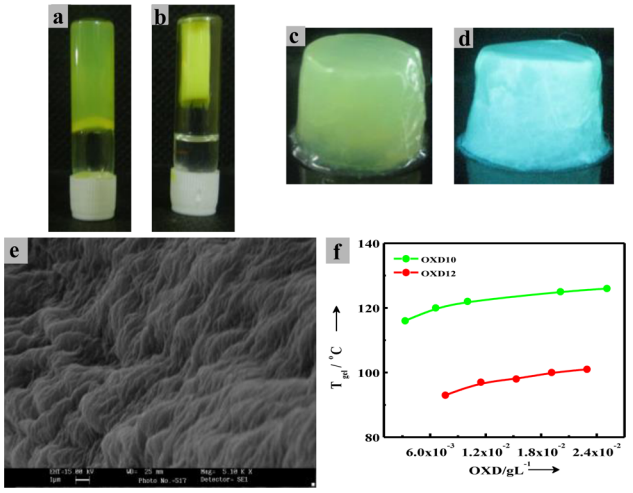

Figure 2. Photographs of OXD12 gel in *n*-decane (1×10^{-2} M) (a) freshly prepared and (b) after a time interval of 12 h. Photographs of OXD10 gel (1×10^{-2} M) at room temperature under (c) normal light and (d) UV (λ_{ex} = 365 nm) illumination. (e) SEM image of OXD10 xerogel. (f) Plots of T_{gel} versus concentration of the OXD gelators in *n*-decane (dropping ball method; wt of ball = 46.55 mg).

istics of the gel formed by OXD10 and OXD12 in *n*-decane. An unusual phase transition was observed for OXD12 gel with time. On letting the gel stand for a period of 12 h, a significant amount of the trapped solvent was squeezed out of the gel as a result of shrinkage of the gel into a small cylindrical mass indicating a secondary level of self-organization. The shrunken gel was highly stable and self-supporting (Figure 2a,b).

The thermal stability of the gels increased slightly with increasing concentration (Figure 2f); with the gels formed from OXD10 showing unusually higher thermal stability compared to earlier reported systems.[9]The super gelating capacity of OXD10 gel in *n*-decane was also evident from the formation of self-standing gels. Reports of such self-standing gels in the literature are rare. Apart from metal−organic hybrids[10] and polymers,[11] earlier reported low molecular weight gelators capable of forming such self-standing gels normally possess strong hydrogen bonding units such as polypeptides[12] and sugars.[13] OXD10 forms a unique example in which the molecule does not possess strong hydrogen-bonding units. Because of the unique stability of the gel it could be cast into any shape (Figure 2c,d). The SEM micrographs of the dry gels (Figure 2e) of OXD10 obtained from *n*-decane exhibited typical images of gel networks consisting of entangled fibers.

TEM image (Figure 3a) of OXD10 at a concentration of 2×10^{-5} M in toluene clearly indicated formation of intertwined

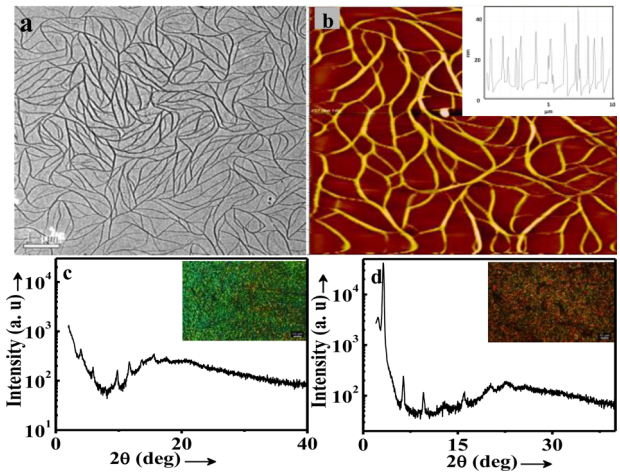

Figure 3. (a) TEM and (b) AFM images obtained for OXD10. Samples were prepared by drop casting from toluene solution at a concentration of 2×10^{-5} M. The inset depicts the height profile of corresponding AFM image. XRD pattern of (c) OXD10 and (d) OXD8 in their xerogel state. The inset depicts corresponding OPM textures obtained for OXD10 and OXD8.

fibers with each fiber possessing a diameter ranging from 15 to 30 nm. AFM analysis was also carried out to confirm this morphology. A film of OXD10 was prepared by drop casting 2×10^{-5} M solution in toluene to a mica sheet, evaporated, and analyzed (Figure 3b). The height profile of fibers obtained by AFM image was very much supportive for TEM images. The AFM and TEM images obtained are further supported by SEM and fluorescence microscopic studies.

The structures of the dry gels were generally investigated by XRD,[14] and the XRD pattern obtained for OXD12 xerogel film showed more reflections, indicating almost crystalline nature of the film. This could be attributed to strong interaction between the neighboring molecules (Table S3). The XRD patterns obtained are shown in Figure 3c,d for OXD10 and OXD8, respectively. The OXD10 xerogel showed reflection peaks at 42.70, 30.91, 22.08, 14.89, 9.02, 7.58, 6.48, 5.68, 4.99, 4.46, and 3.34, and the reciprocal *d*-spacing ratios follow the order $1:1/\sqrt{2}:1/2:1/\sqrt{7}$ which are clearly indicative of a columnar arrangement of the molecules within the nanofibers.

In the case of OXD8, the reflection peaks obtained are 37.94, 27.75, 13.89, 9.26, 6.83, 5.54, 4.38, and 3.93, and the large number of reflection in the low angle region indicates the formation of a columnar arrangement in the xerogel state. The columnar arrangement in the nanofibers was also confirmed by the birefringent textures[15] obtained by OPM investigations. A scheme representing the formation of supramolecular aggregates in the higher homologue of OXD series is expressed in Scheme 1.

The elastic response of OXD10 gel was estimated using rheological measurements.[16] The storage modulus (G') and loss modulus (G'') were determined as a function of applied stress at constant angular frequency for a 1×10^{-2} M solution of OXD10 in *n*-decane. The results of a strain−sweep experiment at a temperature of 27 °C with an angular frequency of 10 Hz, shown in Figure 4a, indicate the value of G' being significantly higher compared to G'' pointing to the dominant elastic nature of the gel. The dynamic moduli, G' and

dx.doi.org/10.1021/ja500607d | J. Am. Chem. Soc. 2014, 136, 5416−5423

Scheme 1. Schematic Representation for the Hierarchical Formation of the Self-Standing Gel of OXD10

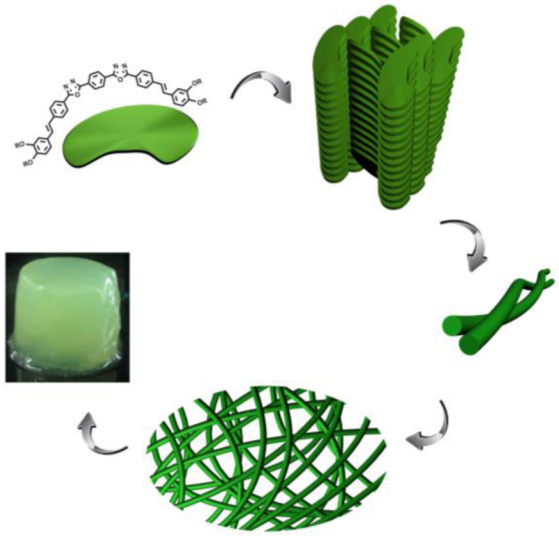

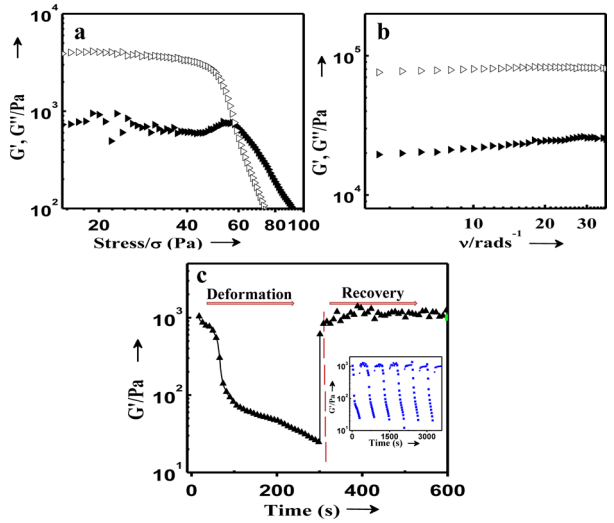

Figure 4. Dynamic moduli, G' (slanted, open triangle) and G'' (slanted, solid triangle), vs strain on double logarithmic scale for a gel of OXD10 (1×10^{-2} M) in *n*-decane at 27 °C with (a) stress = 0.1–100 Pa, angular frequency, ω = 10 Hz and (b) stress = 1 Pa. (c) Thixotropic nature of OXD10 (1×10^{-2} M) in *n*-decane at 27 °C. (Deformation: stress: 0.1 to 100 Pa, time: 300 s, angular frequency, ω = 10 Hz; Recovery: Stress: 1 Pa, time: 300 s; angular frequency, ω = 10 Hz.) (c, inset) Six continuous cycles of measurement for OXD10 gels (1×10^{-2} M) to prove that gel is thixotropic.

G'' remained unchanged until a particular stress value of 57 Pa. Above this yield stress (σy) value, G' and G'' decreased abruptly leading to collapse of gel. Figure 4b shows G' and G'' as a function of angular frequency (ω) at a temperature of 27 °C in the linear viscoelastic regime of Figure 4a, i.e., at a stress value of 1 Pa and the dynamic moduli are invariant over a wide range of strain, indicating a strong solid-like nature of the gel under large deformations.

The thixotropic nature of OXD10 gel was also studied by monitoring the recovery of the destroyed gel. For this process, the gel sample was examined by two continuous processes, i.e. deformation and recovery.[17] In the deformation step, the gel was subjected to a continuously varying stress from 0.1 to 100 Pa at an angular frequency of 10 Hz for 300s. In the recovery process, the storage modulus G' and loss modulus G'' was monitored as a function of time for a low shear stress of 1 Pa at the same angular frequency (10 Hz). This experiment was repeated six times and the results are summarized in Figure 4c. From the Figure it is very clear that the gel recovered immediately after removing the applied stress.

Temperature-dependent ^{1}H NMR studies of OXD10 in solution were conducted in order to understand the nature of the strong intermolecular aromatic $\pi-\pi$ stacking leading to the formation of the strongly self-assembled systems.[18] Temperature-dependent ^{1}H NMR experiments of 1.1 mg/mL solution of OXD10 in toluene, showed slight downfield shifts of the resonance signals for the aromatic protons on the central benzyl ring with decrease in temperature from 70 to 20 °C. As shown in Figure 5, the aromatic central benzyl ring proton

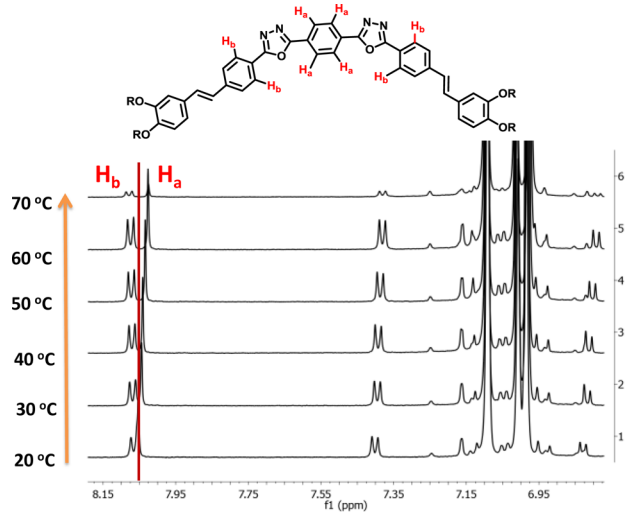

Figure 5. Temperature-dependent ^{1}H NMR spectra of 1.1×10^{-3} M OXD10 in toluene.

signal of OXD10 at 8.02 (s, J = 8.61 Hz, H_a) at 70 °C undergoes a downfield shift to 8.056 (s, J = 8.61 Hz, H_a; ($\Delta\delta$ = 0.036)) finally merging with the H_b doublet upon cooling to 20 °C. On cooling the solution self-aggregation can take place; NMR studies indicate that as a result of interaction between the neighboring molecules in the aggregates, there is a decrease in electron density around the central benzene ring. This can happen when the central benzene ring of the OXD10 molecule interacts with the electron-deficient oxadiazole moiety of the neighboring molecule in the self-assembled system. Such a donor–acceptor type interaction between the neighboring molecules could be the source of strong $\pi-\pi$ stacking observed in the self-assembled materials.

The absorption and emission properties of the OXD derivatives were studied in solvents of varying polarity (Table S4). The photophysical properties of the derivatives were nearly identical, with a strong absorption band centered around 370 nm which was relatively insensitive to solvent polarity and a broad emission band which underwent a red-shift with increasing solvent polarity (Figure S5). The fluorecence quantum yields were very high (0.5–0.8) in the various solvents studied. The fluorescence quantum yield of the OXD10 gel in *n*-decane was estimated as 0.39 using an integrated sphere.

dx.doi.org/10.1021/ja500607d | J. Am. Chem. Soc. 2014, 136, 5416–5423

Since the OXD derivatives showed a strong tendency to form aggregates in nonpolar solvents, their absorption and emission properties as a function of concentration in *n*-decane were studied (Figure 6a). A relative increase in intensity of the

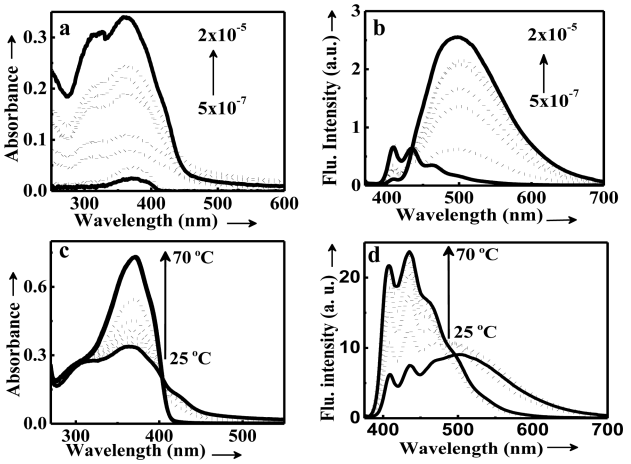

Figure 6. (a) Absorption and (b) emission spectra of OXD10 in *n*-decane (λ_{ex} = 360 nm) with increase in concentration from 5×10^{-7}, 1×10^{-6}, 2×10^{-6}, 4×10^{-6}, 6×10^{-6}, 8×10^{-6}, 1×10^{-5}, and 2×10^{-5} M. (c) Absorption and (d) emission spectra of OXD10 in *n*-decane ($c = 1 \times 10^{-5}$ M; λ_{ex} = 360 nm) with increase in temperature from 25, 30, 35, 40, 45, 50, and 70 °C.

shorter wavelength band was observed with increase in concentration, with a distinct shoulder band being observed at 325 nm for concentrations $\geq 2 \times 10^{-5}$ M indicating the formation of H-type aggregates at higher concentrations.[19] At low concentrations (5×10^{-7} M) the emission showed structured peaks in the 400−470 nm region characteristic of the molecular emission. With increasing concentration the intensity of this band decreased, and this was accompanied by formation of a broad red-shifted emission band attributable to the formation of aggregates (Figure 6b). In contrast the concentration-dependent absorption and emission study of the simple stilbenoid precursor 3e (Scheme S1) did not show any evidence for aggregate formation (Figure S7).

The formation and break-up of the aggregates as a function of temperature was also studied. Figure 6c,d shows the effect of temperature on the absorption and emission spectra of 1×10^{-5} M solution of OXD10 in *n*-decane. At 70 °C, a sharp intense absorption peak was observed with a maximum centered at 370 nm attributable to the monomer absorption (Figure 6c). A decrease in temperature leads to a reduction in the intensity and broadening of the absorption band. The emission of 10^{-5} M solution of OXD10 in *n*-decane at 70 °C showed intense structured peaks in the 400−470 nm region which is characteristic of the molecular emission (Figure 6d), and upon cooling, the intensity of these bands decreased and a new broad red-shifted band centered at 510 nm attributable to the aggregate was observed.

In order to explore the nature of the aggregates formed, a matrix scan experiment of OXD10 at varying concentrations was conducted (Figure 7a,b). Fluorescence spectra were recorded at excitation wavelengths between 280 and 500 nm. As seen in Figure 7a, at low concentrations (5×10^{-7} M), the emission arises from excitation of the monomer band in the 340−400 nm region. Figure 7b shows the recorded emission intensities of 1×10^{-5} M OXD10. From the figure it can be

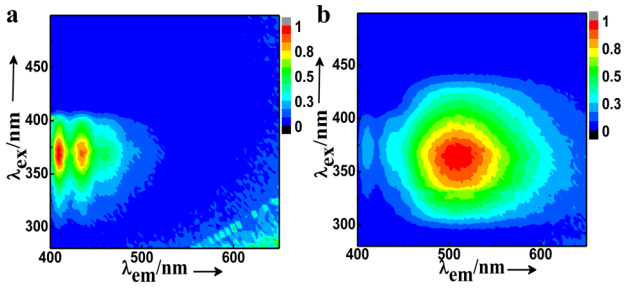

Figure 7. Contour map of the observed fluorescence intensity as a function of the fluorescence excitation and emission wavelength for (a) 5×10^{-7} M and (b) 1×10^{-5} M of OXD10 in *n*-decane.

clearly seen that the emission arises predominantly from excitation of the H-type aggregates and monomeric species. Although H aggregates are generally known to be non-luminescent, there have been a few reports on fluorescent H aggregates in the literature.[20−23] As described above, the pseudodisc-shaped chromophores of OXD10 organize in a columnar fashion within the fibers due to strong $\pi-\pi$ interactions which is conducive to formation of H-type aggregates. The strong intermolecular interactions between the neighboring molecules within the aggregates could lead to rigidization of the chromophores leading to suppression of the nonradiative decay channels.[21] The unusual red-shifted emission from the H-type aggregates observed in these systems may be attributed to an H-to-J coupling as reported earlier for some merocyanine dyes[22] and a few other systems.[23] Such an H-to-J coupling was also clearly observable in the concentration-dependent absorption, emission, and matrix scan experiments of the lower homologue, OXD4 (Figure S6).

■ CONCLUSIONS

In summary, we report a series of 1,3,4-oxadiazole molecules (OXD series, Chart 1) exhibiting columnar super structures both in liquid crystalline and self-assembled nanofibers state. In this series of molecules, OXD10 and OXD12, which possess longer alkyl substituents, exhibited capabilities of forming self-standing gels with very high thermal and mechanical stability in nonpolar solvents. Such an unusually strong supergelating property in molecules which do not possess any hydrogen-bonding motifs and is driven purely by π-stacking interactions of the constituent molecules has hitherto not been observed. Based on temperature-dependent NMR and XRD studies of the gel and the mesophase, the unusual stability of OXD10 gels could be ascribed to the combined effect of aromatic $\pi-\pi$ stacking and the columnar arrangement of molecules in the gel fibers.

■ EXPERIMENTAL SECTION

The solvents and the reagents were dried and purified by standard methods prior to use. The solvents and the reagents were dried and purified by standard methods prior to use. Melting points were determined with a Mel-Temp-II melting point apparatus and are uncorrected. FT-IR spectra were recorded on an IR Prestige-21 Shimadzu FT-IR spectrometer. ^{1}H (300 and 500 MHz) and ^{13}C NMR (125 MHz) spectral analysis were performed on a Bruker Avance DPX spectrometer with TMS as internal standard. The coupling constant values (J = 16 Hz) of the olefinic protons in ^{1}H NMR spectrum of all derivatives confirmed the *E* stereochemistry of the derivatives. HRMS analysis was obtained from a JEOL JM AX 505 HA instrument. Electronic absorption spectra were recorded on a Shimadzu UV-3101 PC NIR scanning spectrophotometer, and emission spectra were

dx.doi.org/10.1021/ja500607d | J. Am. Chem. Soc. 2014, 136, 5416−5423

recorded on a SPEX-Fluorolog FL-1039 spectrofluorimeter. Optical absorption measurements were carried out using 1 or 10 mm cuvettes with a thermistor directly attached to the wall of the cuvette holder for controlling the temperature. Fluorescence quantum yields, with an estimated reproducibility of ±10%, were determined using the standard procedure by comparison with 9,10-diphenyl anthracene in cyclohexane (Φ_F = 1) and 10-methylacridiniumtriflouro methanesulphonate in water (Φ_F = 0.99) as fluorescence standards.[24] Absolute quantum yield in the gel state was measured using a calibrated integrating sphere in a SPEX fluorolog FL-1039 fluorimeter.[25]Fluor-Fluorescence lifetimes were measured using IBH (FluoroCube) time correlated picoseconds single photon counting (TCSPC) system. Solutions were excited with a pulsed diode laser (<100 ps pulse duration) at a wavelength of 375 nm (NanoLED-11) with a repetition rate of 1 MHz. The detection system consisted of a microchannel plate photomultiplier (5000U-09B, Hamamatsu) with a 38.6 ps response time coupled to a monochromator (5000 M) and TCSPC electronics [data station hub including Hub-NL, NanoLED controller, and preinstalled Fluorescence Measurement and Analysis Studio (FMAS) Software]. The fluorescence lifetime values were obtained using DAS6 decay analysis software. For SEM measurements, samples were drop cast and air-dried on flat surface of mica sheet and subjected to thin gold coating using JEOL JFC-1200 fine coater. The probe was inserted into JEOL JSM-5600 LV scanning electron microscope for taking photographs. TEM measurements were carried out in JEOL 100 kV HRTEM. The samples were prepared by drop casting 25 μL of 2 × 10^{-5} M onto a carbon-coated copper grid, and solvent was allowed to evaporate under vacuum. AFM images were recorded under ambient conditions using NTEGRA Prima-NT-MDT, Russia, scanning probe microscope operated in tapping mode. Microfabricated silicone cantilever tips (NSG 20) with a resonance frequency of 260−630 kHz and a force constant of 20−80 N m^{1-} were used. The tip curvature radius was 10 nm. The scan rate was 1 Hz. The AFM samples were prepared by drop casting 2 × 10^{-5} M solution onto a mica sheet, and solvent was allowed to evaporate under vacuum. Liquid crystalline phase transitions and optical anisotropy were observed using a Leica DFC 490 polarized light optical microscope, equipped with a Mettler Toledo FP82HT (temperature programmer) heating and freezing stage. Differential scanning calorimetric experiments were performed using a Perkin-Elmer Pyris 6 DSC instrument in sealed aluminum pans under nitrogen flow, at a heat/cooling rate of 5 °C/min. The rheological investigations were carried out in Physica Modular Compact (MCR 150) stress controlled rheometer from Anton Paar with a cone-and-plate geometry (CP 50-1). XRD studies of xerogel were carried out on samples coated in glass slide, and temperature-dependent XRD studies at liquid crystalline phases were carried out on samples filled in Lindemann capillaries and were held at required temperatures using a Mettler hot stage and irradiated with CuKα radiation (λ = 1.5418 Å). The apparatus essentially involved a high-resolution X-ray powder diffractometer (PANalytical X'Pert PRO) equipped with a high-resolution fast detector, PIXCEL.

■ ASSOCIATED CONTENT

Supporting Information

Synthesis, mesomorphic properties, optimized structures of OXD derivatives in bow and fully extended direction, photophysical properties, temperature-dependent XRD data in the mesophases of OXD derivatives, XRD data in xerogel state, CGCs of OXD derivatives in various organic media, and morphological investigation. This information is available free of charge via the Internet at http://pubs.acs.org/

■ AUTHOR INFORMATION

Corresponding Authors

sureshdas@niist.res.in

skprasad@csmr.res.in

Notes

The authors declare no competing financial interest.

■ ACKNOWLEDGMENTS

Dedicated to Professor C. N. R. Rao on the occasion of his 80th birthday. This work is supported by Council of Scientific and Industrial Research (CSIR) under the Project NWP 55. A.P.S., D.D.P., S.V., N.S.S.K., are grateful to CSIR for fellowships. This is contribution no. NIIST-PPG-349. The authors thank Dr. J. D. Sudha for the rheological studies and Dr. C. N. Ramachandran, Assistant Professor, IIT Roorkee for theoretical calculations.

■ REFERENCES

(1) (a) Lehn, J.-M. *Proc. Natl Acad. Sci. U.S.A.* **2002**, *99*, 4763. (b) Meazza, L.; Foster, J.; Fucke, K.; Metrangolo, P.; Resnati, G.; Steed, J. *Nat. Chem.* **2013**, *5*, 42. (c) Whitesides, G.; Boncheva, M. *Proc. Natl Acad. Sci. U.S.A.* **2002**, *99*, 4769. (d) Whitesides, G.; Grzybowski, B. *Science* **2002**, *295*, 2418.

(2) (a) Camerel, F.; Bonardi, L.; Schmutz, M.; Ziessel, R. *J. Am. Chem. Soc.* **2006**, *128*, 4548. (b) Diring, S.; Camerel, F.; Donnio, B.; Dintzer, T.; Toffanin, S.; Capelli, R.; Muccini, M.; Ziessel, R. *J. Am. Chem. Soc.* **2009**, *131*, 18177. (c) Faramarzi, V.; Niess, F.; Moulin, E.; Maaloum, M.; Dayen, J.-F.; Beaufrand, J.-B.; Zanettini, S.; Doudin, B.; Giuseppone, N. *Nat. Chem.* **2012**, *4*, 485. (d) Huang, Z.; Lee, H.; Lee, E.; Kang, S.-K.; Nam, J.-M.; Lee, M. *Nat. Commun.* **2011**, *2*, 459. (e) Kato, T.; Mizoshita, N.; Kishimoto, K. *Angew. Chem., Int. Ed.* **2005**, *45*, 38. (f) Pisula, W.; Feng, X.; Müllen, K. *Adv. Mater.* **2010**, *22*, 3634. (g) Ziessel, R.; Pickaert, G.; Camerel, F.; Donnio, B.; Guillon, D.; Cesario, M.; Prangé, T. *J. Am. Chem. Soc.* **2004**, *126*, 12403. (h) Keizer, H. M.; Sijbesma, R. P. *Chem. Soc. Rev.* **2005**, *34*, 226. (i) Hashimoto, M.; Ujiie, S.; Mori, A. *Adv. Mater.* **2003**, *15*, 797. (j) Seo, S.; Park, J.; Chang, J. *Langmuir* **2009**, *25*, 8439.

(3) (a) Babu, S.; Prasanthkumar, S.; Ajayaghosh, A. *Angew. Chem., Int. Ed.* **2012**, *51*, 1766. (b) Hirst, A.; Escuder, B.; Miravet, J.; Smith, D. *Angew. Chem., Int. Ed.* **2008**, *47*, 8002. (c) Lara, A.; Lia, A.; Steve, W.; Andrew, D. *Org. Biomol. Chem.* **2004**, *2*, 137. (d) Lee, K.; Kang, M.; Zhang, S.; Gu, Y.; Lodge, T.; Frisbie, C. *Adv. Mater.* **2012**, *24*, 4457. (e) van Bommel, K.; Stuart, M.; Feringa, B.; van Esch, J. *Org. Biomol. Chem.* **2005**, *3*, 2917. (f) Yoshiyuki, O.; Kazuaki, N.; Masahito, S.; Junichi, H.; Seiji, S. *J. Mater. Chem.* **2001**, *11*, 2412.

(4) (a) Abu Bin, I.; Takahiro, S.; Yukikazu, T. *Polym. J.* **2010**, *42*, 839. (b) Harada, A.; Kobayashi, R.; Takashima, Y.; Hashidzume, A.; Yamaguchi, H. *Nat. Chem.* **2011**, *3*, 34. (c) Yamamoto, T.; Yoshida, M. *Langmuir* **2012**, *28*, 8463. (d) Yuichiro, K.; Yoshinori, T.; Akihito, H.; Hiroyasu, Y.; Akira, H. *Sci. Rep.* 2013, *3*. (e) Zhang, M.; Xu, D.; Yan, X.; Chen, J.; Dong, S.; Zheng, B.; Huang, F. *Angew. Chem., Int. Ed.* **2012**, *51*, 7011.

(5) (a) Steed, J. W. *Chem. Commun.* **2011**, *47*, 1379. (b) Buerkle, L. E.; Rowan, S. J. *Chem. Soc. Rev.* **2012**, *41*, 6089.

(6) Shinto, V.; Nambalan, S. S. K.; Anjali, K.; Doddamane, S. S. R.; Subbarao Krishna, P.; Suresh, D. *Adv. Funct. Mater.* **2009**, *19*, 2064.

(7) Lutfor, M.; Yusoff, M.; Tschierske, C.; Pelz, K.; Baumeister, U.; Silong, S. *electronic-Liquid Crystal Communications* **2005**, *28*, 1.

(8) (a) Jing, L.; Panli, H.; Junlin, Y.; Xiaohua, F.; Junxia, P.; Kaiqiang, L.; Yu, F. *Adv. Mater.* **2008**, *20*, 2508. (b) Yoshida, R. *Adv. Mater.* **2010**, *22*, 3463. (c) Murata, K.; Aoki, M.; Nishi, T.; Ikeda, A.; Shinkai, S. *J. Chem. Soc., Chem. Commun.* **1991**, 1715.

(9) (a) De, M.; van, J.; Stokroos, I.; Kellogg, R. M.; Feringa, B. L. *J. Am. Chem. Soc.* **1997**, *119*, 12675. (b) Koevoets, R.; Versteegen, R.; Kooijman, H.; Spek, A.; Sijbesma, R.; Meijer, E. *J. Am. Chem. Soc.* **2005**, *127*, 2999.

(10) (a) Suman, S.; Kumar, B. *Chem. Mater.* **2012**, *24*, 1165. (b) Wang, Q.; Mynar, J.; Yoshida, M.; Lee, E.; Lee, M.; Okuro, K.; Kinbara, K.; Aida, T. *Nature* **2010**, *463*, 339.

(11) Zubarev, E. R.; Pralle, M. U.; Sone, E. D.; Stupp, S. I. *Adv. Mater.* **2002**, *14*, 198.

(12) (a) Mahler, A.; Reches, M.; Rechter, M.; Cohen, S.; Gazit, E. *Adv. Mater.* **2006**, *18*, 1365. (b) O'Leary, L.; Fallas, J.; Bakota, E.; Kang, M.; Hartgerink, J. *Nat. Chem.* **2011**, *3*, 821.

(13) (a) Di, G.; Min, X.; Junxia, P.; Jing, L.; Ni, Y.; Panli, H.; Yu, F. *Tetrahedron* **2010**, *66*, 2961. (b) Kenji, Y.; Natsuki, A.; Yoshiyuki, O.; Tetsuyuki, A.; Hideyuki, S.; Masayuki, T.; Seiji, S.; David, N. R. *Chem.—Eur. J.* **1999**, *5*, 2722. (c) Vidyasagar, A.; Handore, K.; Sureshan, K. *Angew. Chem., Int. Ed.* **2011**, *50*, 8021.
(14) (a) Binglian, B.; Haitao, W.; Hong, X.; Fenglong, Z.; Beihong, L.; Xiaobing, Z.; Songnan, Q.; Min, L. *New J. Chem.* **2007**, *31*, 401. (b) Geo San, L.; Byung Mun, J.; Seung Ju, L.; Hyun Hoon, S.; Chulhee, K.; Ji Young, C. *Chem. Mater.* **2007**, *19*, 460. (c) Nayak, M.; Kim, B.-H.; Kwon, J.; Park, S.; Seo, J.; Chung, J.; Park, S. *Chem.—Eur. J.* **2010**, *16*, 7437. (d) Prabhu, D.; Kumar, N. S.; Sivadas, A.; Varghese, S.; Das, S. *J. Phys. Chem. B* **2012**, *116*, 13071.
(15) Yagai, S.; Kinoshita, T.; Higashi, M.; Kishikawa, K.; Nakanishi, T.; Karatsu, T.; Kitamura, A. *J. Am. Chem. Soc.* **2007**, *129*, 13277.
(16) Huang, X.; Terech, P.; Raghavan, S.; Weiss, R. *J. Am. Chem. Soc.* **2005**, *127*, 4336.
(17) (a) Cai, X.; Liu, K.; Yan, J.; Zhang, H.; Hou, X.; Liu, Z.; Fang, Y. *Soft Matter* **2012**, *8*, 3756. (b) Hou, X.; Gao, D.; Yan, J.; Ma, Y.; Liu, K.; Fang, Y. *Langmuir* **2011**, *27*, 12156.
(18) (a) Feng, Y.; Liu, Z.-T.; Liu, J.; He, Y.-M.; Zheng, Q.-Y.; Fan, Q.-H. *J. Am. Chem. Soc.* **2009**, *131*, 7950. (b) Wu, J.; Fechtenkötter, A.; Gauss, J.; Watson, M.; Kastler, M.; Fechtenkötter, C.; Wagner, M.; Müllen, K. *J. Am. Chem. Soc.* **2004**, *126*, 11311.
(19) (a) Khairutdinov, R. F.; Serpone, N. *J. Phys. Chem. B* **1997**, *101*, 2602. (b) Spano, F. *Acc. Chem. Res.* **2010**, *43*, 429.
(20) (a) Johannes, G.; Larry, L.; Begoña, M.-M.; Dieter, O.; Hans-Joachim, E. *J. Phys. Chem. Lett.* **2013**, *4*, 2686. (b) Verma, P.; Pal, H. *J. Phys. Chem. A* **2013**, *117*, 12409. (c) Vinod, K.; Gary, A. B.; Siddharth, P. *Chem. Commun.* **2011**, *47*, 4730. (d) Zeena, S.; Thomas, K. G. *J. Am. Chem. Soc.* **2001**, *123*, 7859. (e) Nambalan, S. S. K.; Varghese, S.; Suresh, C. H.; Nigam, P. R.; Das, S. *J. Phys. Chem. C* **2009**, *113*, 11927.
(21) (a) Alexandre, F.; Marc, D. J.; Todor, G. D.; Nikolai, I. G.; Aleksey, A. V.; Eric, V. *J. Am. Chem. Soc.* **2006**, *128*, 7661. (b) Cigáň, M.; Donovalová, J.; Szöcs, V.; Gašpar, J.; Jakusová, K.; Gáplovský, A. *J. Phys. Chem. A* **2013**, *117*, 4870. (c) Fang, Q.; Wang, F.; Zhao, H.; Liu, X.; Tu, R.; Wang, D.; Zhang, Z. *J. Phys. Chem. B* **2008**, *112*, 2837. (d) Lau, V.; Heyne, B. *Chem. Commun.* **2010**, *46*, 3595.
(22) (a) Rösch, U.; Yao, S.; Wortmann, R.; Würthner, F. *Angew. Chem., Int. Ed.* **2006**, *45*, 7026. (b) Liangde, L.; Rene, J. L.; Thomas, L. P.; Jerry, P.; David, G. W. *J. Am. Chem. Soc.* **1999**, *121*, 8146.
(23) (a) Seong-Jun, Y.; Jong Won, C.; Johannes, G.; Kil Suk, K.; Moon-Gun, C.; Dongho, K.; Soo Young, P. *J. Am. Chem. Soc.* **2010**, *132*, 13675. (b) Seong-Jun, Y.; SooYoung, P. *J. Mater. Chem.* **2011**, *21*, 8338. (c) Jiajia, C.; Yan, L.; Song, H.; Chang, L.; Liancheng, Z.; Xianshun, Z. *Chem. Commun.* **2013**, *49*, 6259.
(24) (a) Weber, G.; Teale, F. W. J. *Trans. Faraday Soc.* **1957**, *53*, 646. (b) Jonker, S. A.; Ariese, F.; Verhoeven, J. W. *Recl. Trav. Chim. Pays Bas* **1989**, *108*, 109.
(25) (a) John, C. d. M.; Wittmann, H. F.; Richard, H. F. *Adv. Mater.* **1997**, *9*, 231. (b) Pålsson, L. O.; Monkman, A. P. *Adv. Mater.* **2002**, *14*, 757.